

Dependence of Retinal Ganglion Cells' Responses to Natural Images on the Mean Contrasts of the Receptive-Field Center and Surround

Xiwu Cao^{1,2}, David K. Merwine³, and Norberto M. Grzywacz^{1,2,4,5}

1. Department of Biomedical Engineering, University of Southern California
2. Center for Vision Science and Technology, University of Southern California
3. Division of Biological and Health Sciences, University of Pittsburgh at Bradford
4. Department of Electrical Engineering, University of Southern California
5. Neuroscience Graduate Program, University of Southern California.

Authors, Mailing Address, Telephone Number:

Xiwu Cao, 1042 Downey way, DRB 140, Los Angeles, CA, 90089, 310-254-0551

David K. Merwine, Division of Biological and Health Sciences, 203D Fisher Hall, University of Pittsburgh at Bradford, Bradford, PA 16701, 814-362-5126, dkm14@pitt.edu.

Norberto M. Grzywacz, 1042 Downey way, DRB 140, Los Angeles, CA, 90089. 1-213-821-1150, nmg@bmsr.usc.edu

Short Title: Center and Surround of RGCs with Natural Images

Abstract

Properties of natural images are different from those of the artificial stimuli typically used in studying visual receptive fields (RFs). Here, we report on the center and surround properties of retinal-ganglion-cell (RGC) RFs when stimulated by natural images. In particular, we focus on response dependence on their local mean contrast, that is, on their first-order statistics. We isolated rabbit retinas and recorded RGC responses with multi-electrode arrays by alternating natural images with homogeneous, full-field gray stimuli. To these responses, we first applied a new method for estimating the sizes of the RF center and surround from natural images. We found that center sizes estimated with our method were similar to those obtained with standard artificial stimuli and that RGCs' responses increased sigmoidally with the mean contrast of the receptive field center. Further analysis revealed that natural images were encoded sparsely, since little or no response was elicited in any given RGC by most of them, and cells rarely got saturated. In addition, with natural images, the mean contrast of the center area of the RF was a strong predictor of the RGC's responses. Its inhibitory surround showed a weak dependence on mean contrast. The average response reduction due to inhibition rarely exceeded 30% for the largest mean surround contrasts. Our data showed that the reason for the sparseness, absence of saturation, and weak dependence of surround inhibition on mean contrast was the low contrasts predominance in natural scenes. In conclusion, RGC RFs appear to keep their basic structures in the mean sense when stimulated by natural images, but the characteristics of their responses strongly depend on the statistical properties of natural scenes.

Keywords:

Rabbit, Retinal ganglion cell, Visual receptive field, Surround inhibition, Natural image, Contrast

Introduction

Receptive fields (RFs) of neurons in the early visual system, *e.g.*, retinal ganglion cells (RGCs), have an antagonistic concentric structure with an excitatory center and an inhibitory surround (Barlow, 1953; Kuffler, 1953; Rodieck, 1965; Levick, 1967; Enroth-Cugell & Lennie, 1975; Amthor et al., 1989; Sagdullaev & McCall, 2005). The center-surround structure is presumed to be very important, since it is found in all invertebrate and vertebrate species studied (Ratliff, 1965; Sagdullaev & McCall, 2005). Several theories attempt to explain this concentric, antagonistic structure. It could behave as a “whitening filter” to decorrelate responses (Srinivasan et al., 1982; Atick, 1992), perform “edge enhancement” to help in the detection of object boundaries (for a brief review, see Balboa & Grzywacz, 2000), maximize the transmission of information (Laughlin, 1981), help constrain energy consumption (Vincent & Baddeley, 2003), or reduce the effect of the illuminant on visual responses (Land, 1959).

Although much research has addressed RGC RF structure, our knowledge of it is based on data collected using artificial stimuli, including flashing spots, drifting gratings, and Gaussian white noise (Reid et al, 1997; Rust & Movshon, 2005). No direct analyses of the center-surround organization of RGCs with natural stimuli are available. One straightforward reason for this is that controlling the stimulation of the center and surround structures individually is difficult with natural images.

Unfortunately, one cannot simply extrapolate RF properties obtained with artificial stimuli to those obtained in the natural environment (Simoncelli & Olshausen, 2001; David et al., 2004; Sterling, 2004; Felsen & Dan, 2005). One obstacle towards extrapolating conclusions to natural images is that visual processing is often nonlinear (Allman et al., 1985; Merwine et al., 1995; Kaplan & Benardete, 2001). In addition, natural images have several special statistical

properties. For example, natural visual stimuli usually contain a high degree of spatial and temporal correlation (Field, 1987; Ruderman & Bialek, 1994; Balboa & Grzywacz, 2003). Moreover, the power spectra of these stimuli tend to fall with the square of spatial frequency (Burton & Moorhead, 1987; Tolhurst et al., 1992; van der Schaaf & van Hateren, 1996; Balboa & Grzywacz, 2003). And the peak of their contrast distribution is at zero, with this distribution falling exponentially with contrast (Field, 1987; Ruderman & Bialek, 1994; Balboa & Grzywacz, 2003). Finally, the distribution of intensities in any given image is such that more points are darker than brighter than the mean (Field, 1987; Ruderman & Bialek, 1994; Olshausen & Field, 2000; Simoncelli & Olshausen, 2001).

Concerns about extrapolating conclusions from those obtained with artificial stimuli are serious, since RGCs appear adapted to these natural statistics. For instance, retinas have more Off cells than On cells (Ahmad et al., 2003; Koch et al., 2006). In another example, the RGCs' contrast sensitivities increase as the square of spatial frequency (Enroth-Cugell & Robson, 1966; Atick, 1992), resulting in a decorrelation of input stimuli. Thus, to understand how RGCs function in natural conditions, one must analyze their RF center and surround properties with natural-image stimulations.

In this paper, we report on some of the properties of RGC center-surround interactions in the natural environment. We first developed a new method to measure center and surround sizes in natural conditions. Then, we looked at the functional relationship between cell responses and the mean contrasts of the center and surround. We focused on mean contrasts, because earlier quantitative studies of center-surround interactions focused on the contrasts of center spots and surround annuli (Merwine et al., 1995). Thus, we could compare our results directly with those obtained with an important class of artificial stimuli. An initial report of the center-surround interactions of RGCs with natural stimuli has appeared in abstract form (Cao et al., 2006).

Methods

Physiological preparation

This preparation was similar to that reported elsewhere (Chatterjee et al., 2007). Briefly, pigmented rabbits weighing between 2 - 4 kg were dark adapted for 30 minutes before beginning surgery. Surgery was conducted under dim red light. All experimental procedures were approved by the Institutional Animal Care and Use Committee (IACUC) at the University of Southern California, in accordance with the Guide for the Care and Use of Laboratory Animals (National Institutes of Health). Rabbits were initially anesthetized with I.P. Ketamine (50mg/kg) and Xylazine (5mg/kg). Then pentobarbital sodium (1ml/kg) was injected into the marginal ear vein to obtain deep anesthesia. Anesthesia was checked by testing corneal reflexes and reactions to a paw pinch. After confirming a lack of reflexive movement, an eye was enucleated and the eyecup was hemisected. The animal was subsequently euthanized with an I.V. overdose of pentobarbital sodium.

The superior retina was gently separated from the pigment epithelium and then mounted, RGC side down, over a hole punched in a Whatman Filter paper. The filter paper was then flipped and mounted in a recording chamber. A metal ring gently held the paper in place. Once in the chamber, we continuously superfused the retina with oxygenated bicarbonate-buffered Ames solution (Sigma) at 37°C at a flow rate of 3-7 ml/min. The isolated retina remained healthy for about 6 hr post isolation

Electrophysiological recording and visual stimulation

Methods of recording from a multi-electrode array (Cyberkinetics) and spike sorting by using a professional software POWERNAP (Cyberkinetics) were as previously described (Chatterjee et al., 2007). So were general methods of visual stimulation, determination of each cell's response polarity (On or Off), temporal property (transient or sustained), and spontaneous firing rate. A total of eight isolated retinas and 102 RGCs were analyzed in this study.

We also modified a technique employed elsewhere to map the RF with artificial stimuli (Rodieck & Stone, 1965). In our modification of that technique, 20 trials of a low spatial-frequency square-wave moving grating (0.14 cycle/mm) were displayed rightwards, leftwards, upwards, and downwards. The spatial frequency of these images was so low that each cell only saw one edge at a time.

In contrast, our natural-image methods are unique to this paper and thus, we describe them here in detail. The natural images used in our study were obtained from the online calibrated-image database at <http://hlab.phys.rug.nl/archive.html> (van Hateren & Ruderman, 1998). We further calibrated them to be linear with respect to our monitor's luminance. The source images with 1536×1024 pixels were cropped down to either their square central regions or into eight evenly spaced regions with 300×300 pixels. Each region was then down-sampled into a square image of 120×120 pixels ($3 \times 3 \text{ mm}^2$ on the retina). Images were presented in a random sequence, each for 1000 ms. When the natural image was removed, the display was held at a spatially uniform gray for 1000 ms before the next image was presented. The mean intensities of the gray and natural images were the same (9.10 cd/m^2) to remove luminance adaptation. The long periods of presentation of gray and natural images allowed us to distinguish clearly between responses to onset and offset of the images (Smyth et al., 2003). We presented from 1,000 to 12,000 images in different experiments.

Data analysis

Contrast in natural images

The contrasts of a natural image with respect to an RGC's RF center and surround area (to be specified in the next section) are defined respectively by

$$C_c = \frac{M_c - M_{gray}}{M_{gray}} \quad (1)$$

$$C_s = \frac{M_s - M_{gray}}{M_{gray}} \quad (2)$$

where M_c is the mean intensity of the specified center area, M_s is the mean intensity of the specified surround area, and M_{gray} is the mean intensity of full-field gray, which is the same as the mean of entire natural image. The center and surround areas are determined with our new method based on cross-correlation (third method in the next section). The definition of contrast in this study is different from the traditional root-mean-square (RMS), where the contrast is defined as the ratio between the standard deviation of pixel intensities and their mean (Peli, 1990). The reason we did not use the RMS definition is that it captures only spatial contrast in a single area (*e.g.*, the RF center or the RF surround). Hence, the RMS contrast in a region could be zero in both the gray and the natural images, even if the mean intensity changed between them. In other words, the RMS contrast does not capture temporal contrast or relative spatial contrast between neighboring regions. Instead, one can view C_c or C_s as temporal contrast, *i.e.*, the change between the gray and natural images. Alternatively, one can view them as the spatial contrast, representing the relative difference between the center (or surround) and the entire image.

Receptive-field-center estimation

An accurate measurement of the RF center and surround areas is important for properly interpreting how each contributes to cell responses. We estimated the RF center of each cell with three different approaches.

1. RF estimate from moving a square-wave grating in four directions.

This approach uses the square-wave grating drifting in four orthogonal directions as described in the last section. When an edge with appropriate contrast polarity moves into the RF of a cell, a response begins. That moment minus the response delay, if mapped into space, indicates the boundary of the cell's RF center (Rodieck & Stone, 1965). The delay is the time difference between the beginning of full-field step and the cell's subsequent response. Time delays estimated in our experiments varied across cells with a maximum of about 200 ms and a mode of 35 ms. Therefore, by moving a square-wave grating of low spatial frequency across the RF in the four cardinal directions, we could quickly sketch the RF center. This RF-mapping-with-motion approach is similar to the "minimum discharge field" of Hubel & Wiesel (1962). The histograms of one cell's responses to all four directions are shown in Figs. 1A-D. To visualize the two-dimensional RF obtained from moving the square-wave grating, we used its speed to scale the histogram from time (ms) into space (μm) (insets of Figs. 1 A-D). Finally, we combined the spatial mapping of all directions to get a rough approximation of the cell's RF center (Fig. 1E).

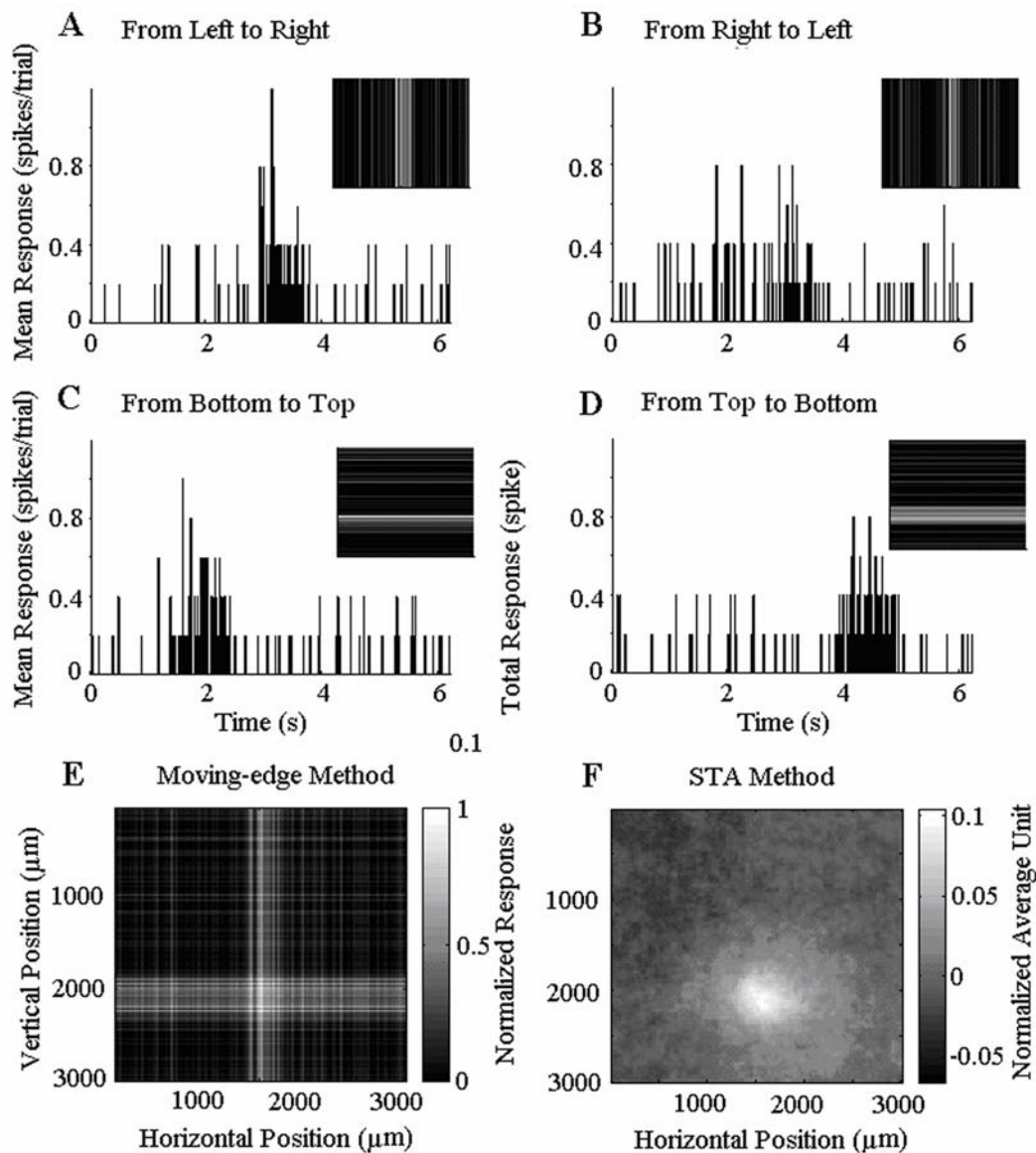


Fig. 1. Fast sketch of an On brisk transient RGC's RF with both a drifting square-wave grating and STA of natural images. A low spatial-frequency square-wave grating (0.14 cycle/mm) was displayed drifting in four directions: rightwards (A), leftwards (B), upwards (C), and downwards (D). The post-stimulus time histograms of responses for each grating direction for 20 trials were scaled into the spatial position by taking grating velocity and response delay into account as shown in the insets. E. Receptive-field approximation from the combination of the insets in A-D. F. Receptive-field estimation of the same RGC as in E from STA of natural images.

2. RF estimate from natural images based on spike-triggered average (STA)

A rough estimation of the RF from natural stimulation can be obtained by using the spike-triggered average (STA – Willmore & Smyth, 2003). This estimation would be valid if we assumed the RGC to be linear and the input to be white noise (Marmarelis & Marmarelis, 1978). The estimation would also be correct if the system could be modeled as a linear-followed-by-static-nonlinearity system with either Gaussian white noise (Chichilnisky, 2001; Willmore & Smyth, 2003) or some other orthogonal stimulus as input (Reid & Alonso, 1995; Ringach et al., 1997). However, natural images are neither white nor orthogonal. They have considerable spatial (and for movies, temporal) correlations. Usually, a further normalization by the autocorrelation matrix of natural images had to be implemented to correct for these spatial and temporal correlations (Theunissen et al., 2000; Smyth et al., 2003; Willmore & Smyth, 2003; Calvetti & Reichel, 2004). Nevertheless, these techniques only consider second-order correlations between pixels in natural images and require these correlations to be stationary. We used these techniques understanding their limitations. An RF estimated with STA is shown in Fig. 1F. Although the RF estimated with STA from natural images is larger than that derived from the moving grating, their positions match well.

3. RF estimate from natural images based on cross-correlation between responses and putative RFs

We proposed a new method to estimate the RF center based on one of our discoveries from natural stimulation and the ubiquitous concentric structures of RGCs. In our experiments, we found that the center mean contrast was a strong predictor of a cell's responses when stimulated with natural images, even if we varied the assumed center size over a quite large range. Concomitantly, the surround influence was weak compared to the center. We know that

traditionally, the RF center is defined as the area where one can elicit a cell's response, and the surround is the region that can modulate a center-elicited response. Therefore, in our study, we assumed that the correct center should be the region where we could obtain the maximal cross-correlation coefficient between the cell's response and the center mean contrast of the natural images. The cross-correlation coefficient is

$$C(C_c, r) = \frac{\sum (C_c - \bar{C}_c)(r - \bar{r})}{\sqrt{\sum (C_c - \bar{C}_c)^2 \sum (r - \bar{r})^2}} \quad (3)$$

where r is the cell's response to an image, \bar{r} is the mean responses across all images, C_c is the center mean contrast of an image, \bar{C}_c is the mean of center mean contrasts across all images, and the summations are over all images (Aertsen, et al., 1989).

Figure 2 illustrates this method to determine RF center size from natural images. Let us assume that the light gray disc represents the actual RF center and the black disc represents the actual RF surround. We make various guesses of what the center may be (white disks). When the guessed center size is small compared to the actual center size (Fig. 2A), the correlation coefficient between the guessed-center mean contrasts and the cell's responses will be relatively small. This is because this guessed center only considers a part of the influence from the actual center. As the guessed center size approaches the correct center size, the cross-correlation coefficient will increase. When the guessed center size is correctly selected, a maximal correlation coefficient is reached (Fig. 2B). A further increase in the guessed center size will lower the strength of correlation (Fig. 2C). This is because the guessed center will mistakenly assign some surround influences to the center. Consequently, the trend of the correlation coefficients should behave as an inverted U-shape function as we continuously vary the guessed

center size from small to large (Fig. 2D). The radius that maximizes this function is our estimate of the radius of the RF center.

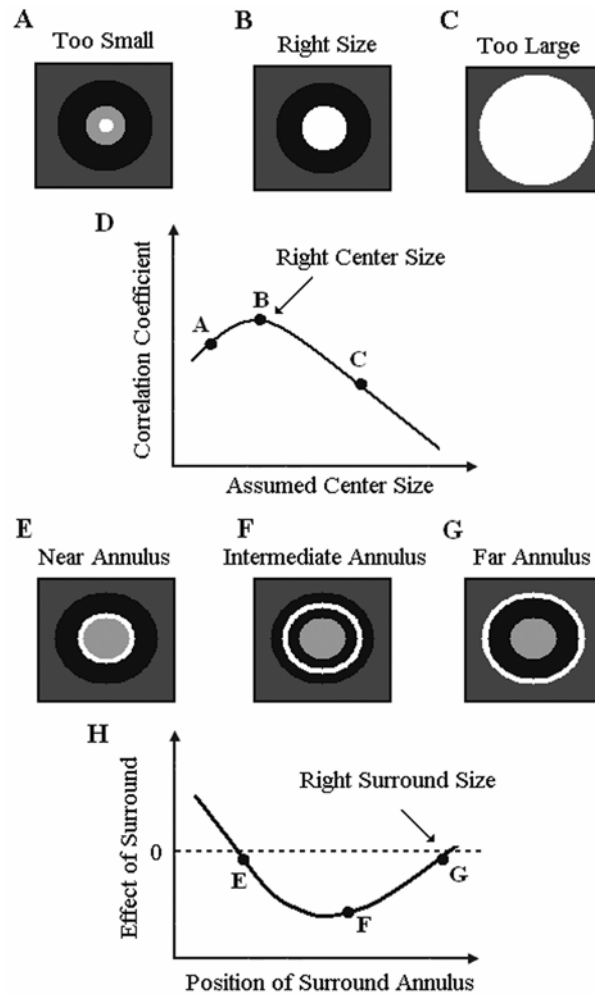


Fig. 2. Methods for determining the RF center and the surround size from natural images. In this figure, the light gray and black discs represent the true RF center and surround areas respectively. In turn, the white discs represent guesses for RF center sizes and the white annuli represent testing windows for the surround. A. If the guessed RF center size is small compared to the true center size, then the correlation between the center mean contrasts and responses will not be maximal (D). This is because some areas of the true center are missed. B. If the guessed RF center size is correct, then the correlation is maximal (D). C. If the guessed RF center size is larger than the true center size, the correlation will also fail to be maximal (D), because the guessed center includes some areas of the surround. We estimate the RF center

size from Point B of the resulting bell-shape curve (D). After we estimate the true center size, we split the surround into many mutually exclusively annuli. We then check how the mean contrasts within these annuli influence responses. For a cell with inhibitory surround, when the positions of the annulus vary from closest (E) to farthest (G), the surround will show inhibition (H). Near Position E, inhibition may be weak (H), as some excitatory influence from the RF center contributes to responses. Near Position G, inhibition may be weak (H), as the surround is ending. Thus, some intermediate position (F, H) will yield maximal inhibition. We estimate the surround size from Position G of the resulting U curve (H).

Receptive-field-surround estimation

While the center region is the place that elicits cell's responses, the surround region is the area that modulates these responses, typically, in an inhibitory manner. We took advantage of this modulation to devise a method to estimate the size of RF surround. After we estimated the center size, we split the area outside the center into many mutually exclusive probing annuli (white annuli in Figs. 2E-G). For each annulus, we calculated the surround mean contrast (Eq.2) within this annulus. We then considered those images with similar center mean contrast (Eq.1). Because the center mean contrast was the same, any systematic response variations would depend on the changes of surround mean contrast. Practically, only very few images were available when center mean contrast was fixed. Hence, we selected a segment of center mean contrasts, which would introduce the response interference from the center mean. To remove it, we first characterized the center-mean-contrast contributed responses based on a cumulative Gaussian distribution curve (see next section), and then subtracted them to obtain the responses contribution from the surround. A straight line was then fit to quantify the function between the responses and surround mean contrasts. We took the slope of this line as a measure of the surround effect. Positive and negative slopes indicate excitation and inhibition respectively. For

a cell with an inhibitory surround, all annuli within the surround area, from the closest annulus (Fig. 2E) to the farthest annulus (Fig. 2G), will show inhibition. At one position, the inhibition strength will reach a maximum negative value (Fig. 2F). As we continuously vary the probing surround annulus from closest to the center to the farthest (Fig. 2H), the trend of inhibition strength will thus be a U-shape function. When the probing annulus is just too large, this function returns to zero, as the annulus should cause no inhibition. The surround size is thus determined by that point of this U-shape function, shown as Point G on Fig. 2H.

We determined the strength of the surround only for cells that yield a clear U-shape behavior as in Fig. 2H (39 neurons in our sample). Only for those cells could we be certain where the surround begins and ends. The estimation of the surround strength used stimuli between Points E and G of Fig. 2H. The inner radius would ideally be at the border of the RF center, not at Point E. However, this point, which came from the first annulus eliciting inhibition, had often a larger radius. This is because annuli near the border of the RF center will have some excitatory contributions from the center. This contribution is due to the spatial correlation of natural image stimuli. In other words, we could classify these annuli as neither center nor surround. Thus, in the estimation of inhibitory strength, we used as inner radius that defined by the first annulus eliciting inhibition. The details of the methods used to determine strength will appear in **Results**.

Contrast-response function estimation

To investigate the dependence of each cell's responses on the RF center's mean contrast, we fitted the contrast-response function with a cumulative-Gaussian-distribution curve (Chichilnisky, 2001). A cumulative Gaussian distribution curve is defined by

$$r = \frac{A}{2} \left[1 + \operatorname{erf} \left(\frac{C_c - M}{\sigma\sqrt{2}} \right) \right] \quad (5)$$

where A is the maximal firing rate, M is the contrast value of the maximum slope, and σ is the standard deviation of the Gaussian distribution. A criterion of minimum mean-squared error was applied to obtain an optimal estimate.

Results

Polarity of RF with natural-image stimulation

Our goal in this work was to study how the center and surround of RGCs interact when stimulated with natural images. To undertake this study, we first had to find out what basic features of a natural image caused RGCs to respond. Based on the experiments with artificial stimuli, we expected RGCs to respond to spatio-temporal contrasts. For instance, we expected On and Off RGCs to respond best when the mean intensity of natural images increased and reduced in their RF center, respectively. As Fig. 3 illustrates, RGCs meet this expectation. The polarity (On or Off) of an RGC as established with artificial stimuli remained the same when one stimulated these cells with natural images.

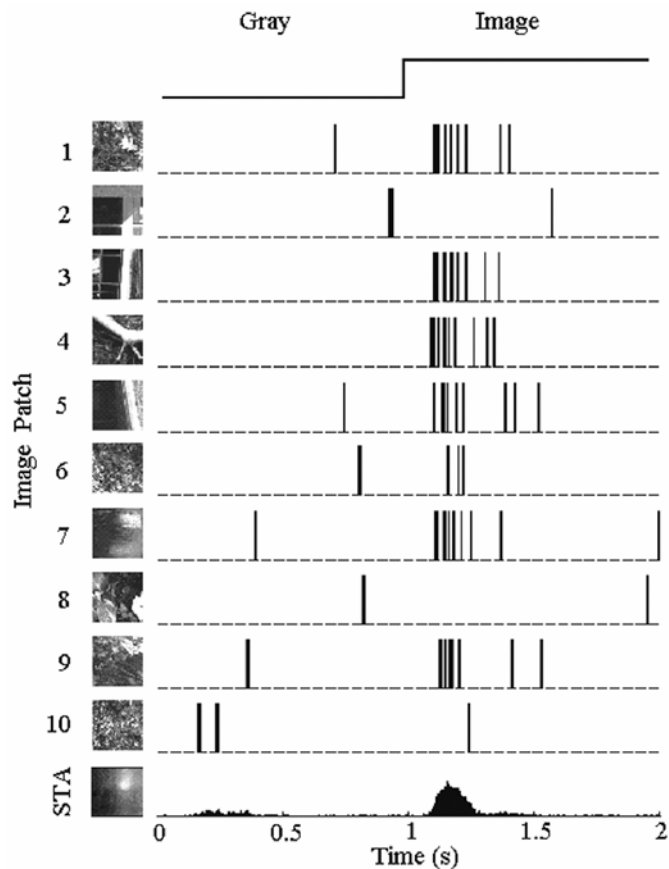


Fig. 3. Example of one On brisk transient RGC’s responses to natural images. Ten patches of natural images are shown on the left-hand side of each row, along with their responses on the right-hand side. The bottom row displays the RF estimated from STA of 1000 natural images and the post-stimulus time histogram of the RGC’s responses. This On RGC yields large responses when bright regions stimulate its RF (Image Patches 1, 3, 4, 5, 7, and 9), and yields low responses otherwise (Image Patches 2, 6, 8, and 10).

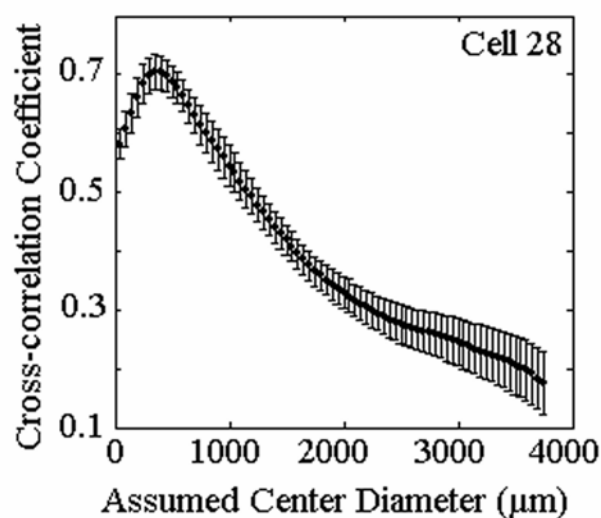
An example of On cell (as established with full-field steps) responses to natural images is shown in Fig. 3. A rough estimation of the RF center based on STA (**Methods**) using 1,000 natural images appears in the bottom of the figure. The other ten rows show the responses of this cell to exemplar natural images. This cell responded strongly to natural images when a bright region stimulated its RF center (Rows 1, 3, 4, 5, 7, and 9). In contrast, the cell responded poorly

when images were not bright in the RF center (Rows 2, 6, 8, and 10). We found similar responses with other On cells and the inverse polarity with Off cells. Figures like those thus lead to the conclusion that cells keep their polarity with natural stimuli. Moreover, such figures illustrate that the STA is a rough but simple method to determine the RF center with natural images.

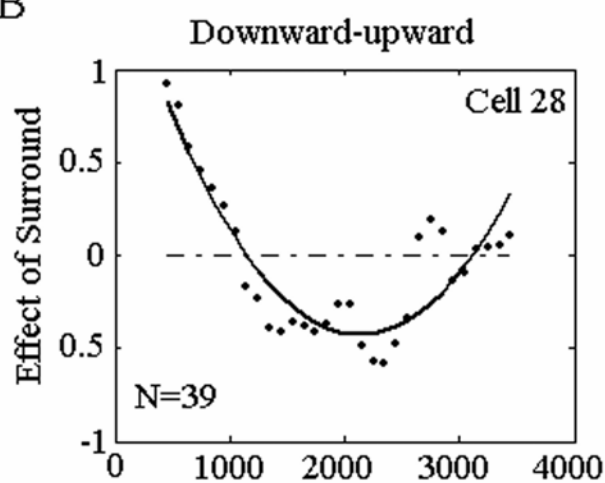
Estimation of RF-center size with natural-image stimulation

One reason that the STA only provides rough estimates of RF centers is that it assumes linear cellular mechanisms, whereas RGCs exhibit spatio-temporal nonlinearities (**Introduction**). Furthermore, STA works best with uncorrelated inputs, which is not the case with natural images (**Introduction**). We thus devised a new method to estimate RF center size with natural images (Fig. 2A-D). We used this method, aided by an estimation of the RF center location with STA. Results appear in Fig. 4.

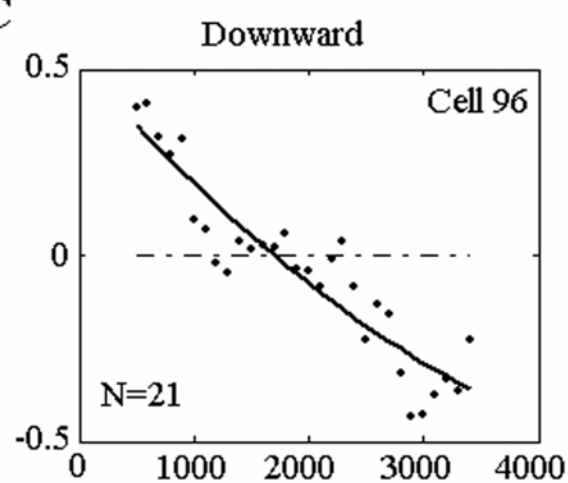
A



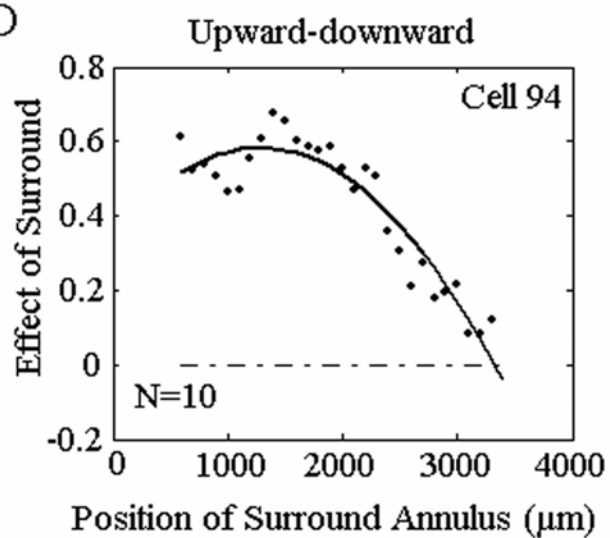
B



C



D



E

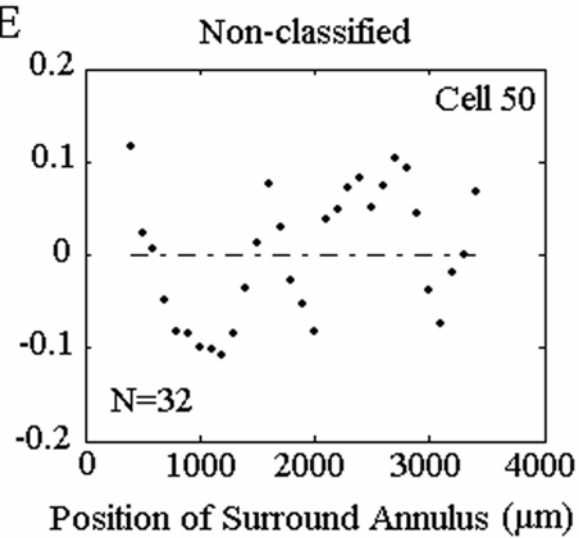


Fig. 4. Using natural images to estimate RF center size and classify surround behaviors. A. The RF center was estimated with the method illustrated in Figs. 2A-D by using the cross-correlation coefficient. Error bars stand for one standard error, based on jackknife analysis with 90% data and 10 groups (Efron and Tibshirani, 1993). With cross-correlation coefficient, the diameter of the RF center was estimated around 400 μm for the example RGC in this figure (an Off sluggish sustained RGC). In turn, we observed four different types of RF-surround behavior when using the methods of Figs. 2E-H: B. Example of an Off sluggish sustained RGC (same cell as Fig. 4A) exhibiting the downward-upward (U-shape) effect of surround as a function of annulus position predicted in Fig. 2. C. Example of a downward-only function (for an On sluggish transient RGC). D. Example of an upward-downward function (for an On-Off brisk transient RGC). E. Example of an On-Off brisk transient RGC whose behavior was not classified in one of the above three categories. Of the 102 cells recorded, we had 39 RGCs with downward-upward trends, 21 cells with downward trends, 10 cells with upward-downward trends, and 32 non-classified cells (N values inside panels). See text for the interpretation of these four types of trends.

Figure 4A shows respectively for one cell how the cross-correlation (Eq. 3) between the responses and the mean contrasts vary with guessed RF center diameter. As predicted in Fig. 2, Fig. 4A has an inverted U-shape function. The estimation of RF center diameter is around 400 μm for this cell. All cells reported here showed inverted U-shape functions with the cross-correlation technique.

To confirm the validity of the cross-correlation technique for RF-center estimation, we compared it with two alternate methods. The first alternative was STA and the second used the square-wave gratings moving in four directions (**Methods**). For comparison, we selected an On cell (Fig. 5A) and an Off cell (Fig. 5B) to illustrate the RF estimated with the three different methods. For each cell, the left panel illustrates the RF center sketched from the moving-grating

technique. In turn, the right panel illustrates the RF estimated from STA of natural-image stimulation. The RF center determined with the cross-correlation method is shown as the red ring in both panels. One can see that the method based on cross-correlation captures well the center size estimated with the moving gratings. The center area estimated with STA is not too different, but as predicted, larger than obtained with the other methods.

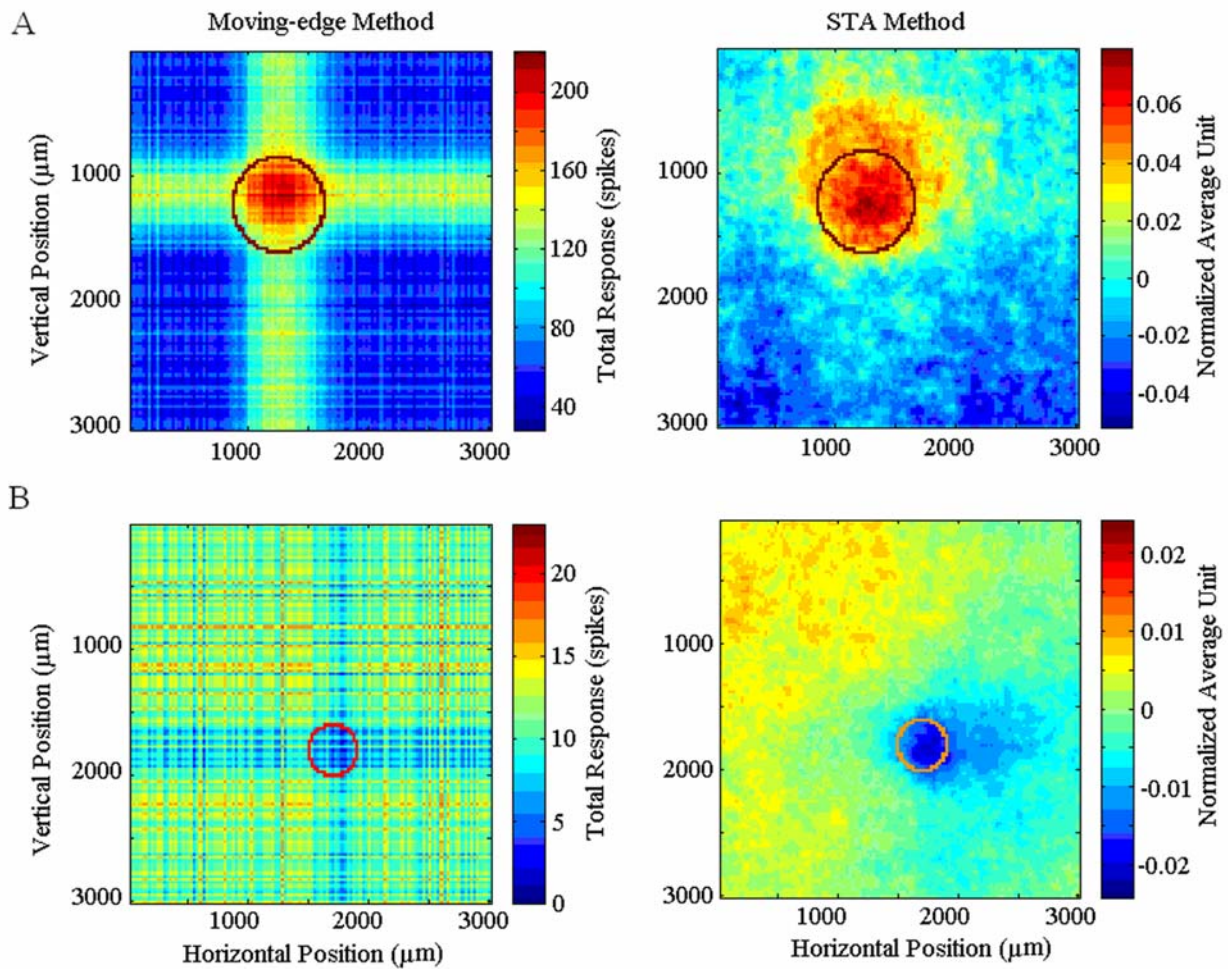


Fig. 5. Comparison of RF center-size estimation with three different methods, one with artificial and two with natural images. Panels A and B give RF examples for an On RGC and an Off RGC respectively. The left hand-side of each panel is the RF center sketched from the moving-grating method (Fig. 1E). The right hand-side is the RF estimated from STA of natural images (Fig. 1F). The RF center estimated

from cross-correlation of natural images (Fig. 4A) is plotted as the red rings. The method based on cross-correlation yields similar RF center sizes as those from moving gratings. However, STA overestimates the RF centers, because of the spatial correlation between neighboring regions in natural images.

With a sample of thirty-three cells, we compared the center sizes estimated from moving gratings with those estimated from natural images using the cross-correlation method (Fig. 6A). The methods based on artificial and natural stimuli yielded strongly correlated estimates of center size. The cross-correlation coefficient between the center sizes estimated with these two methods was 0.87. In conclusion, our cross-correlation method is a valid, robust technique to estimate RF-center size from natural images.

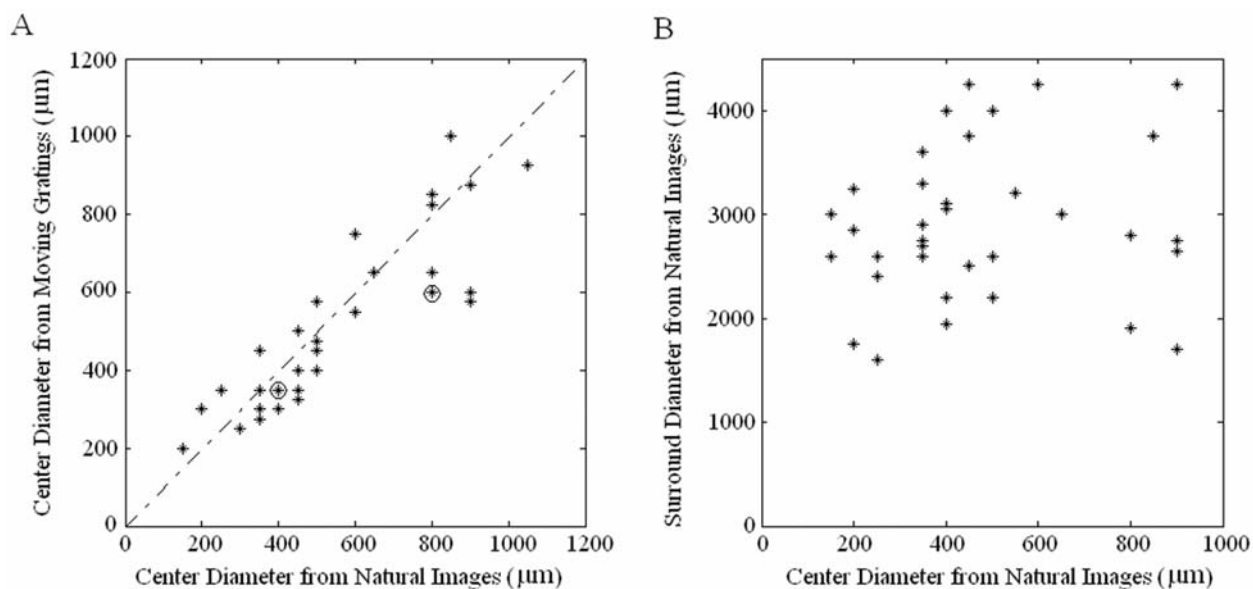


Fig. 6. Distribution of RF center and surround sizes. A. Center sizes estimated with moving artificial gratings versus those estimated with natural images based on the cross-correlation method. Each point shows a single cell’s RF-center size estimated with both methods. Only those RGCs with clear boundaries in response to moving gratings are included. The two example cells illustrated in Fig. 5 are marked with the open circles. The center sizes estimated with the cross-correlation method are similar to those estimated with moving gratings, with diameters exhibiting a positive correlation coefficient of 0.87.

B. Distribution of RF-center and surround sizes estimated with natural images based on the cross-correlation method. Here, only those RGCs with the surround downward-upward trend are considered (Fig. 4B). We do not include the other RGCs, because we cannot determine their surround sizes based on our method.

Estimation of RF-surround diameter with natural-image stimulation

After we obtained the RF center, we estimated the RF surround. The surround is the region that modulates the cell's responses from the center. For estimating the RF surround, we split the area outside the RF center into many mutually exclusively annuli (Figs. 2E-G). We then considered images with fixed center mean contrast and measured how the surround mean contrast within these annuli influenced the responses (Fig. 2H). Results of our use of this multi-annulus technique appear in Figs. 4B-E.

For the cells recorded in our study, four different types of surround behavior were observed. In the first surround type, response went downward and then upward (U-shape) as a function of the distance of the surround annulus from the RF center (Fig. 4B). In the second type, the response went only downward (Fig. 4C). A possible reason for this downward function is that the surround was so large for these cells, that we could not visualize the upward portion of the behavior with the available stimuli. The third surround type yielded an upward-downward behavior (Fig. 4D). This behavior occurs for those cells with a facilitatory, instead of an antagonistic, surround. All other cells that could not be classified into one of the above three categories formed our fourth type. For these types of behavior, we were not certain whether the surround was facilitatory or antagonistic. One example is shown in Fig. 4E. We think that the uncertainties of these cells were mostly due to the surround influence being weak and thus easily corrupted by noise. Hence, we could not observe clear surround behaviors for these cells. In

total, we recorded from 102 cells. From those, we had 39 cells with surrounds displaying downward-upward trends, 21 cells with downward trends, 10 cells with upward-downward trends, and 32 non-classified cells. For the 70 classified cells, the ratio between the number of cells with antagonistic surround (60 cells) and those with facilitatory surround (10 cells) was 6:1.

With data like those in Fig. 4, we could measure and compare the diameters of the RF center and surround. We limited this comparison to the 39 cells with a downward-upward surround trend (Fig 4B). We chose this constraint because these cells had clear zero crossing positions in their surround, allowing us therefore to determine its size. The 10 cells with facilitatory surrounds were not studied in this way, since they were too few in number. We also did not consider the other two categories in Fig. 4. This is because either the surround regions of these cells were beyond the available stimuli or the surround effect was too weak to get a clear estimation of surround boundaries. Results for the comparison of RF center and surround diameters appear in Fig. 6B.

Figure 6A shows that the diameters of the RF centers and surrounds are variable and do not correlate over the population of RGCs. Center diameters for the recorded cells ranged from about 150 to 900 μm . For the same cells, surrounds had diameters between about 1500 to 4000 μm , with the ratios between the surround and center diameters being variable. In the extremes, while the smallest ratios we found were about two, the largest were almost twenty.

We conclude that the basic center and surround structure of the RF revealed by natural images is similar to the structure revealed by artificial ones.

Dependence of responses to natural images on mean contrasts

With artificial stimuli, the stimulus contrasts at the RF center and surround control RGCs' responses (Merwine et al., 1995). To ask whether the same happens with natural images, one

must first define their contrasts over the given regions of the scenes. Natural images have complex structures, making multiple definitions possible. The definitions that we adopted for this investigation could be interpreted as the relative temporal changes of mean intensity in the center (Eq. 1) and in the surround (Eq. 2). Alternatively, one could interpret these definitions as the relative difference of mean intensities between the center (and between the surround) and the rest of the image, since the mean intensity of images were the same as full-field gray. Figure 7A uses a false color scheme to show how responses varied with mean contrasts for an Off-brisk-transient RGC. (To make such figures comparable for On and Off cells, we invert the sign of contrast for the latter in this and all other figures of the paper.) To generate this figure, we first split the entire ranges of center and of surround contrasts into 30 evenly spaced intervals each. Thus, with two variables, center mean contrast and surround mean contrast, we got 900 combinations. For every combination, we calculated the mean response over 1000 natural images.

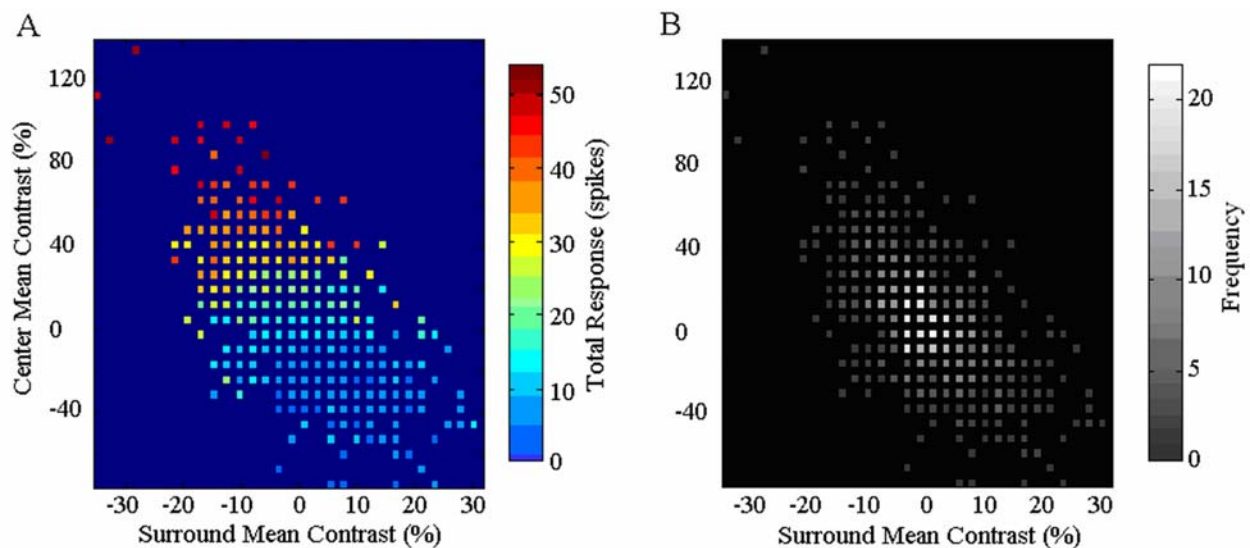


Fig. 7. Response and contrast-frequency distribution for an example Off-brisk-transient RGC stimulated with 1000 natural images. After estimating the RGC's RF center and surround sizes (Fig. 6), we

calculated the center (Eq. 1), and surround (Eq. 2) mean contrasts for all images. To make such figures comparable for On and Off cells, we invert the sign of contrast for the latter in this and all other figures of the paper. We then separated the entire ranges of center and surround contrasts into 30 evenly spaced intervals, getting 900 (30×30) pairs of contrasts. A. Mean responses as a function of center and surround mean contrasts. The graph shows that the center mean contrast dominates the cell's responses, because if one fixes surround contrast, responses vary strongly with center contrast but not vice-versa. B. Joint distribution of center and surround contrasts. This joint distribution peaks at zero and, in our experiments, center and surround contrasts exhibit a negative correlation. (The negative correlation between center mean contrasts and surround mean contrasts in Fig. 7 is an artifact of our choice of images. The mean intensities of our natural images and of the gray images that preceded them were the same. We did so to control for effects of overall intensity modulation. Therefore, if, say, the RF-center intensity in a natural image is above this mean, the peripheral intensity will be below. If the image patches are small, then the surround of the cell will occupy most of the periphery. Consequently, the surround will have a mean intensity below the mean.)

Based on the two-dimensional function plotted in Fig. 7A, the responses increase as the RF-center and RF-surround mean contrasts rise and fall respectively. In this kind of plot, the center mean contrast dominates the responses. With fixed surround mean contrast, the cell's responses vary considerably if we select images such as to modulate the center mean contrast from low to high. Responses can vary from zero to the maximal saturated value that the cell can reach, especially for low surround contrasts. However, if instead we fix the center mean contrast, the cell's responses do not change as much.

Figure 7A does not show how many images exhibit each particular combination of center and surround contrasts. To quantify this point, we plot the joint distribution of center and surround mean contrasts in Fig. 7B. Again, every point represents a particular combination of

center and surround mean contrasts. However, different from Fig. 7A, the gray level in Fig. 7B represents how many natural images had the specified combination of contrasts. The main conclusion from this figure is that most natural images have both low center mean contrast and low surround mean contrast. One rarely observes a natural image with high center or surround contrast. These results are consistent with those of previous studies (Field, 1987; Ruderman & Bialek, 1994; Balboa & Grzywacz, 2003), but this figure extends the conclusion to contrasts in spatial scales similar to those of RGCs' RFs.

Because the center mean contrast controls the cells' responses, we further quantified the dependence of responses on this variable. Figure 8 shows an example of this quantification for the same cell as in Fig. 7. In this figure, small dots are the original responses to 1,000 natural images, which produced the indicated mean contrast in the RF center. Then, we divided the center mean contrasts into 20 equally spaced intervals. We grouped images with center mean contrasts in these intervals to calculate their mean responses. The mean responses are plotted as large dots. The trend of mean responses shows a sigmoidal increase with the center mean contrast of natural images. In addition, Fig. 8 displays the center-mean-contrast distribution (dotted curve). Comparing this distribution with the response dependence on contrast reveals that the majority of natural images cause low responses, and that only a few images lead to response saturation.

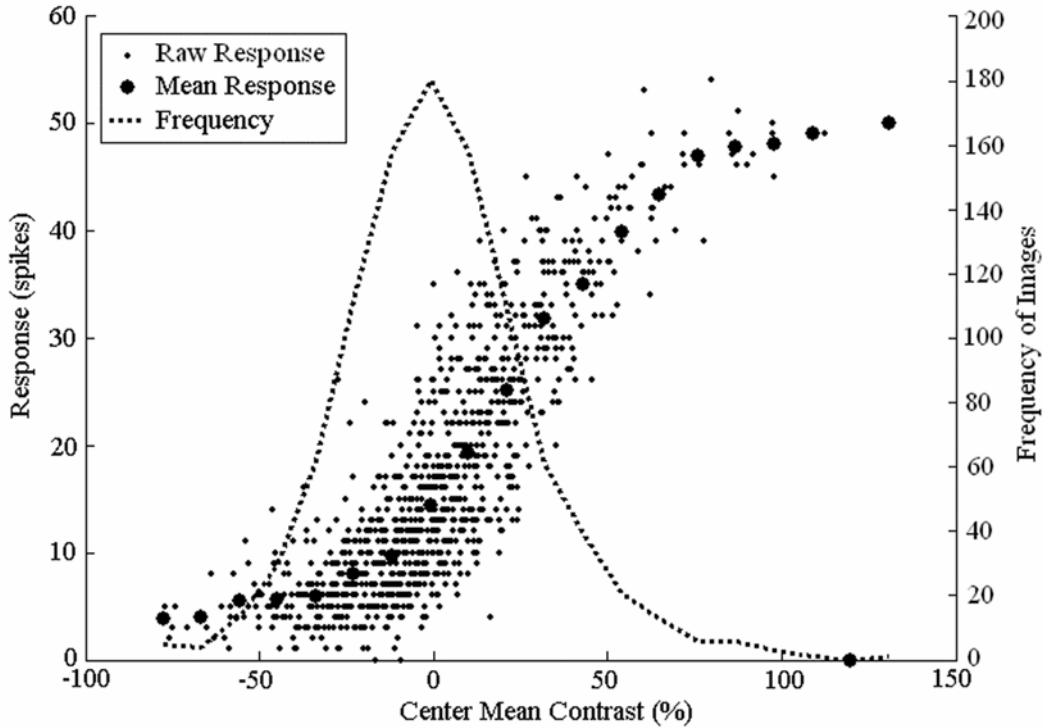


Fig. 8. Responses of an Off brisk transient RGC to 1000 natural images as a function of the center mean contrasts. Pairs of responses and center mean contrasts are plotted as the small dots. We also separated the whole range of center mean contrasts into 20 equal intervals, and calculated the mean responses (large dots). Finally, the dotted curve shows the distribution of center mean contrasts for all images (right vertical axis). The RGC’s responses increase sigmoidally with the center mean contrasts of natural images, but the majority of them cause little response and only rare images cause saturation.

We attempted to fit the sigmoidal behavior of the relationship between response and center mean contrast with a cumulative Gaussian function (Eq. 5). The fit proved to be good, capturing the mean response in each contrast interval (Fig. 9). Figure 9A shows the same cell as in Fig. 8. Figures 9B, 9C, and 9D are three other examples from Off transient, On-Off transient, and Off transient cells respectively. As in Fig. 8, the dotted curves in Fig. 9 show the distribution of center mean contrasts in natural images. The peaks of these distributions were located around -5% to 5%. In turn, the fitted “means” in the cumulative Gaussian-distribution functions

(Parameter M in Eq. 5) were around 25%. Because about half of natural images produce negative center mean contrasts, this percentage confirms that any given cell shows little or no responses to most natural images.

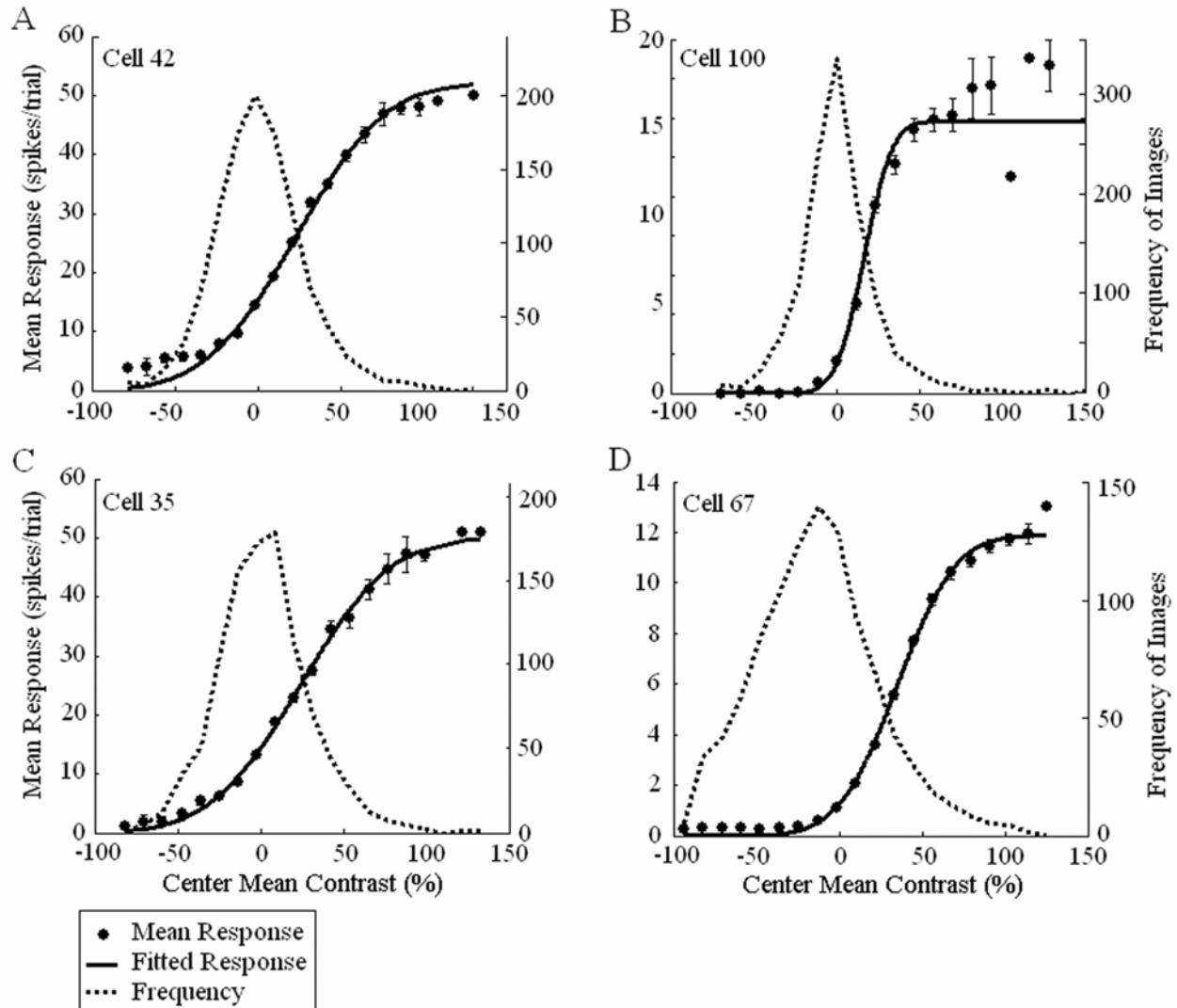


Fig. 9. Examples of four cells to illustrate the sigmoidal relationship between mean responses and center mean contrasts of natural images, and fits of a cumulative-Gaussian-distribution model (Eq. 5). These fits are plotted as solid curves. Large dots show the mean responses in 20 separate intervals of contrasts. The distributions of center mean contrasts are plotted as dotted curves. A. The same RGC as in Fig. 8. B. Example for an On-Off brisk transient RGC. C. Example for an On-Off transient RGC. D. Example for

an Off brisk transient RGC. The cumulative-Gaussian-distribution model provides an excellent fit to the response-contrast curve. The sign of the center mean contrast is inverted for Off cells to simplify comparison with the curves for On cells.

In conclusion, the main variable controlling the responses of RGCs to natural images is the mean contrast in the RF centers and thus, as it tends to be low, these cells produce a sparse encoding of natural stimuli (Vinje and Gallant, 2000; Olshausen and Field, 2004).

Weak surround-inhibition dependence on mean contrast

With artificial stimuli, contrasts in the RF surround tend to inhibit RGCs' responses (Enroth-Cugell & Robson, 1966; Merwine et al., 1995). For example, with annuli, an 80% surround contrast can reduce responses by factors of five or more in the rabbit retina (Merwine et al., 1995). However, as already observed in Figs. 7-9 and elsewhere (**Introduction**), contrasts in natural images are low. Therefore, if surround inhibition depended on mean contrast, one might expect that stimulation with natural images would have much less effect on the surround than the typical artificial stimulation. Furthermore, averaging out luminance variation over the large surrounds of RGCs (Fig. 6B) may exacerbate their weak dependence on mean contrast. Figure 7A had already illustrated that the dependence of surround inhibition on mean contrast was weak. For most center mean contrasts, this figure revealed no effect of the surround. Only around center mean contrasts of 20% we observed an effect of surround. For these center mean contrasts, responses in Fig. 7A yielded yellow and light-blue colors for surround mean contrasts of -15% and 15% respectively. This corresponded to a fall of response by about a factor of two. However, by taking into account other center mean contrasts, we expected that the dependence of inhibition on surround mean contrast to be weaker.

We quantified the strength of surround inhibition of each cell as the percentage change in responses over all natural images in the input set. To estimate this percentage, we grouped those images with suitably pre-selected center mean contrasts. These center mean contrasts were selected to make sure that cells had enough high responses. Therefore, we avoided those negative center mean contrasts because they produced small or no responses (Figs. 7-9). With such small responses, we did not have a large enough range to observe surround inhibition even if it existed. In addition, the selection of the center mean contrast had to provide enough images for statistical reliable estimates, so we did not consider saturating contrasts that happened only for a few images (Figs. 7-9). For these grouped images, we first calculated the center-mean-contrast contributed responses based on the cumulative Gaussian distribution Model (Fig. 8). Then, we obtained the surround-related effects by subtracting the model prediction from the actual responses. Finally, we performed a linear regression of these surround-related effects as a function of surround mean contrasts. We used the percentage of fall between the maximal and minimal values of the regression line over the range of mean surround contrasts to measure the inhibition strength of the surround.

In measuring this strength, we focused on center mean contrasts between 0 and 50%. The result of this analysis over the population of cells appears in Fig. 10A. Since the inhibition strength that we actually calculated was the mean response reduction at the largest contrast, we called it the mean maximal percentage of response reduction. This figure includes the 39 RGCs for which we could determine their inhibitory surround sizes (Fig. 6B). We did not include the 10 RGCs with facilitatory surrounds.

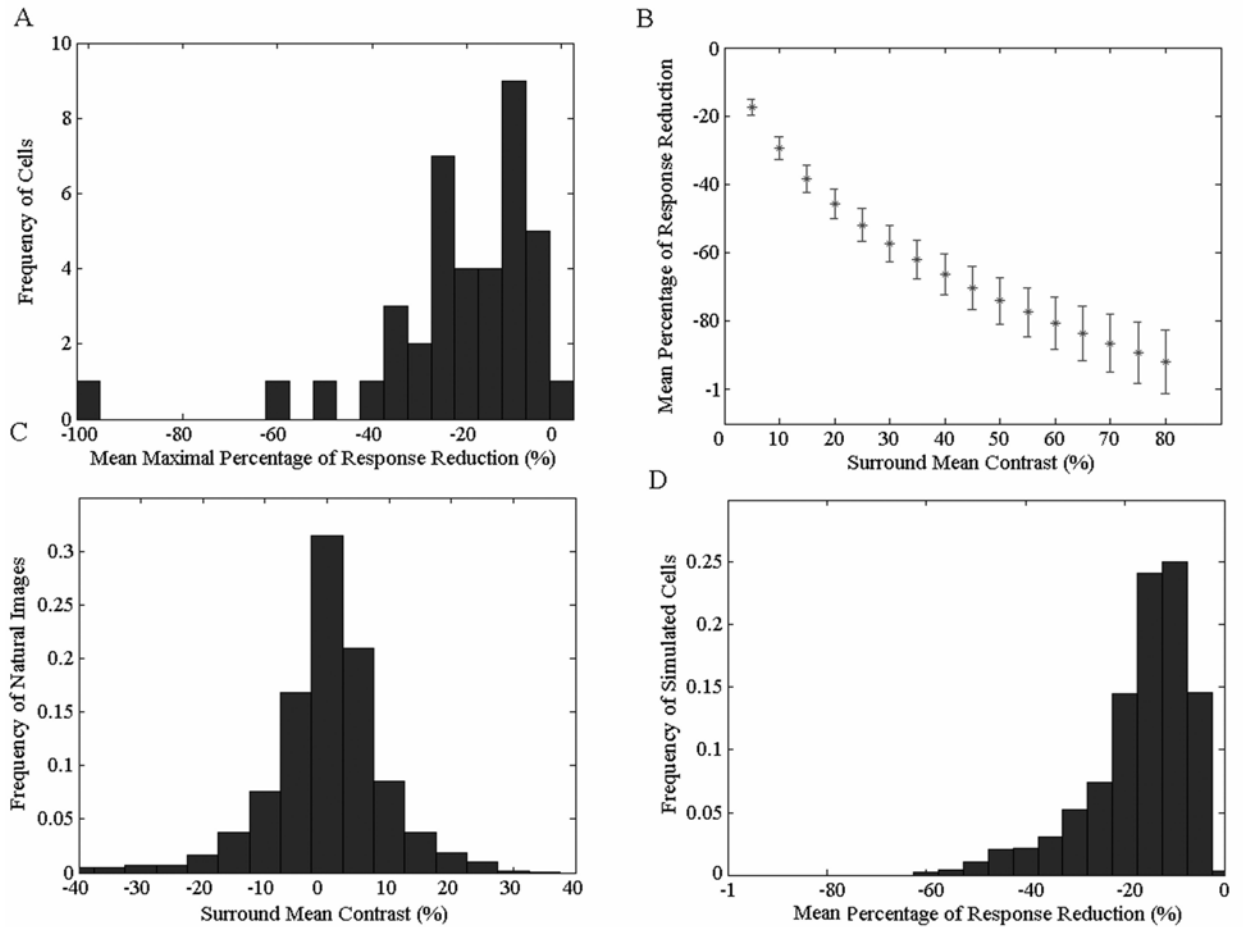


Fig. 10. Mean maximal reduction of response as a function of surround mean contrasts with our sample of natural images. A. Distribution of mean maximal response reductions (due to surround inhibition) of 39 RGCs. This figure includes only RGCs that exhibited the downward-upward surround trend (Fig. 4B). Most natural images elicit mean overall response reductions as a function of surround mean contrast of less than 30%. B. Mean response reduction as a function of surround contrast for the 26 RGCs in Table 1 of Merwine *et al.* (1995). C. Distribution of surround mean contrasts of the RGCs in this paper. D. Distribution of mean response reductions of the 26 RGCs of Merwine *et al.* estimated using the center and surround mean contrasts of natural images reported in this paper (Fig. 1). The similarity of Panels A and D argues that the weak surround inhibition that we observe is not due to a difference in mechanisms when using artificial and natural stimuli. Rather, the weakness is due to the statistics of natural images (Panel C). They yield low surround mean contrasts, which in turn may cause weak inhibition.

Figure 10A shows that the mean maximal reduction of response as a function of surround mean contrast across natural images is typically less than 30%. The median reduction was 15% for all the cells in this figure. Thus, the surround inhibition of RGCs' showed weak dependence on the local mean contrast of natural images.

Why is the mean maximal reduction of responses smaller than 30% for natural images but can reach 80% with artificial annuli? Is this difference due to changes (*e.g.*, adaptation) of the RGCs' RFs with natural images? Or are the RF mechanisms the same, but the properties of natural images explain the apparent weak inhibition? To answer this question, we used the model developed by Merwine *et al.* (1995). It accounts for RGCs center-surround interactions when using spots and annuli (see their Eq. 3).

Figure 10B shows the mean response reduction due to surround inhibition for the 26 RGCs quantified by Merwine *et al.* We plot these mean response reductions as a function of surround mean contrast. These plots are for center mean contrasts of 25%, 50%, and 75%, that is, the same range as in Fig. 10A. As expected, surround inhibition increases as the surround mean contrast rises. The surround-inhibition strength can be above 80% when the surround mean contrast is larger than 50%. However, natural images typically yield surround mean contrasts between -15% and 15%. Figure 10C shows the distribution of surround mean contrasts for a typical RGC with 1,000 natural images. The 39 cells in Figure 10A yield similar distributions of surround mean contrasts. If we use these distributions with the Merwine *et al.* model and their 26 RGCs (for $26 \times 39 = 1,014$ mean response-reduction estimates), then the predicted probability distribution of mean response reductions appears in Fig. 10D. Comparison of this figure with Fig. 10A shows a striking similarity. As in Fig. 10A, the predicted surround inhibition with a model obtained with artificial annuli but natural contrasts also yield mean response reductions mostly below 30%. We thus conclude that the apparent mean maximal response reduction due to

surround inhibition when using natural images is due to the predominance of low contrast in these stimuli.

Discussion

Estimation of RF with natural images

The RF is defined as the region of visual space from where one can elicit responses with light stimuli (Kuffler, 1953). Although this definition is clear, the estimation of the RF is dependent on the stimuli used. For instance, Barlow et al. (1957) showed that the inhibitory surround disappears at low mean background intensities. Here, we asked whether the RF estimated with natural images would be different from that estimated artificially.

The most commonly employed technique for estimating RFs with complex stimuli is STA (Willmore & Smyth, 2003). However, STA has three problems when used with natural images. First, STA requires the system to be linear, or linear-nonlinear (Chichilnisky, 2001; Willmore & Smyth, 2003). Unfortunately, the visual system shows complex nonlinearities, including rectification, saturation, multiplication, and division (Poggio & Reichardt, 1976; Torre & Poggio, 1978; Grzywacz & Koch, 1987; Carandini & Heeger, 1994). Second, STA requires stimuli to be Gaussian white noise. However, natural images are neither white nor Gaussian (Ruderman & Bialek, 1994; Balboa & Grzywacz, 2003). Third, STA cannot separate the center and surround contributions to the RF, but mixes them.

The technique that we developed estimated RF center boundaries without the above limitations (Fig. 2). The main assumption of our technique is that the mean contrast of the RF center is a strong predictor of responses with relatively weak modulation from the surround. This assumption was corroborated by our experiments (Fig. 10A). Another assumption is that the RFs of ganglion cells are roughly circular, which seems to be correct (Kuffler, 1953; Rodieck, 1965; Levick, 1967). With these assumptions, our method yielded a center size similar to that captured by the traditional method with moving square-wave gratings (Fig. 5). In contrast, STA

tended to over-estimate the size of the RF center. One possible explanation for this over-estimation is that the correlation between the RF center and its neighboring area in natural scenes may tend to make the neighboring area artifactually provide a positive contribution to RGCs' responses. Our method avoids this artifact. The success of this method suggests that we can redefine the RF as the region where one obtains the maximal correlation between responses and mean contrasts.

We also devised a method to estimate the RF surround size by seeking those areas outside the center that statistically modulate an RGC's responses, typically in an inhibitory manner (Fig. 2). An alternate method would have been STA if, for example, the interaction between the RF center and surround were linear (*e.g.*, a difference-of-Gaussians), followed by a static nonlinearity (Rodieck & Stone, 1965; Enroth-Cugell & Robson, 1966). However, the center-surround interaction is nonlinear (Enroth-Cugell & Robson, 1966; Carandini & Heeger, 1994; Merwine et al., 1995). Our method does not need to assume a linear interaction between center and surround. However, our technique also has some limitations. First, our method has to assume that the surround is circular, which is only an approximation of the shape of RGC dendritic trees (Rockhill et al., 2002). Second, we estimate only the size of the RF center and surround, rather than the RF itself as STA does. Third, our method ignores the RF spatial weighting function, which may also potentially cause a bias in our estimation.

Contrast dependence of center and surround responses with natural stimuli

When using spots and annuli, the contrasts at the RF center and surround are strong predictors of RGCs responses. We thus organized the responses to natural images according to the mean contrasts in the center and the surround. One can predict the response well from the mean contrast of the RF center (Figs. 7-9). However, organizing the data in terms of mean surround

contrast revealed a weak dependence (Fig. 10). In other words, when organizing the natural-image data according to contrast, the RF center dominates the RGCs' responses.

The dependence of the RGCs' responses on the mean contrast of the RF center leads to interesting consequences. Figs. 8 and 9 reveal that most natural images cause little or no response. Only rare natural images have sufficiently high center mean contrasts to cause cells' responses to saturate. Thus, the retina produces a sparse coding of natural stimuli. Such sparseness is consistent with some cortical models of visual function, which suggests that individual neurons respond rarely but reliably (Vinje & Gallant, 2000; Olshausen & Field, 2004). That we found weak dependence of surround inhibition on mean contrasts of natural images does not mean it was unreliable. We detected surround inhibition in most cells. For the seventy cells for which we could classify the surround (Fig. 4), sixty showed inhibition and only ten showed excitation. Thus, the ratio of RGCs exhibiting an inhibitory surround to those exhibiting a facilitatory surround is approximately 6:1 (Fig. 4). Therefore, as found with artificial stimuli, stimulation of the surround with natural images mostly elicits inhibition.

However, when organizing the data in terms of surround mean contrasts, the surround inhibition elicited by natural images is weak. Maximal mean reduction of responses due to surround inhibition is typically below 30% (Fig. 10). This low reduction is apparently different to what one observes with spots and annuli. With annuli one can routinely observe reductions of 80% or more (Merwine *et al.*, 1995). Why are reductions of responses due to surround inhibition apparently weak when using natural images? One possibility is that perhaps our experiments used relatively low mean luminance. Barlow *et al.* (1957) showed that surround inhibition becomes weak and even disappears when the mean luminance falls. Another possibility was that we used stationary images rather than natural movies. Perhaps, one could argue, strong surround inhibition requires motion. And still a third possibility for the weakness of inhibition is that our

methods did not allow looking for contributions of inhibition in the RF center. However, we used a similar stimulation setup as in the study of Merwine et al. (1995). They could elicit strong surround inhibition ($> 80\%$) with stationary stimuli outside the RF center, using similar photopic background illumination as we did. Hence, the explanation for the apparent weakness of our surround inhibition was neither in low background levels, nor on the lack of motion, and nor in failing to stimulate the center inhibition.

Because surround inhibition can be strong with artificial stimuli, we wondered whether RGCs' RFs adapt to natural-image statistics. Alternatively, RFs could be the same as for artificial stimuli, but stimulated differently due to the special statistics of natural images. Our analysis suggests that the latter alternative is correct (Fig. 10). We propose that the weak dependence of surround inhibition on mean contrasts of natural images is simply due to the surround area of the RF seeing a preponderance of low contrasts (Ruderman & Bialek, 1994; Balboa & Grzywacz, 2003). In addition, surround regions are large, and thus, see much visual texture in natural images. The dark and bright intensities in these textures tend to cancel out, thus causing even lower mean contrasts in the surround than in the center. As shown in Figs. 10 C-D, low contrasts could make surround inhibition apparently weak (Barlow et al. 1957; Merwine et al., 1995; Devries & Baylor, 1997). Thus, the mechanism of surround inhibition itself is probably not weak with natural images.

What may be the function of a 'weak' surround inhibition with natural images? We entertain two broad possibilities. The first is that inhibition is not weak but that statistical moments other than surround mean contrast are what matter. We explored surround mean contrast in this paper, because with annuli, contrast is what matters for surround inhibition. However, annuli have no luminance variation, which may be important for inhibition. A hint that this may be the case is that annuli with negative surround contrasts cause little or no

inhibition (Merwine *et al.* 1995). However, as the data for 20% center mean contrast in Fig. 7 show, with natural images, negative mean surround contrasts have an effect. Therefore, one may uncover stronger inhibition by organizing the data with higher order statistics instead of surround mean contrast. A future study using such high-order statistics is therefore of interest.

A second possibility is not to deny that surround inhibition is weak for natural images and to consider the possible functions of the weakness. All of the functions proposed for surround inhibition so far have been based on it being strong. These proposals include the removal of correlation in the input stimuli (Atick, 1992), predictive coding (Srinivasan *et al.*, 1982), and detection of sharp image transitions (Ratliff, 1965). None of these proposals works well if surround inhibition is weak. As an alternative, we propose that the weakness of the surround inhibition, although not optimal for the above visual functions, may be necessary for maintaining information about the absolute reflectance of large objects or regions in scenes. A strong surround, however, would make points in these large regions inhibit mutually, causing responses to become sub-threshold. As a minimum, we would have to modify the theories above, developed assuming strong surround inhibition, to allow for compromises imposed by it being weak. Another compromise may be to take both energy consumption and information-transformation efficiencies into account, since strong surround inhibition will introduce a strong metabolic cost (Laughlin, 1981; Vincent & Baddeley, 2003).

Acknowledgements

We thank Susmita Chatterjee, Eun-Jin Lee, Junkwan Lee, Mónica Padilla, Joaquín Rapela, and Jeff Wurfel for their helpful discussions of the material, and Denise Steiner for administrative assistance. This work was supported by National Eye Institute grants EY08921, EY11170, and EY016093, and a National Science Foundation grant EEC-0310723 to N.M.G.

References

- Aertsen, A.M., Gerstein, G.L., Habib, M.K. & Palm, G. (1989). Dynamics of neuronal firing correlation: modulation of "effective connectivity". *Journal of Neurophysiology* **61**(5), 900-917.
- Ahmad, K.M., Klug, K., Herr, S., Sterling, P., Schein, S. (2003). Cell density ratios in a foveal patch in macaque retina. *Visual Neuroscience* **20**(2), 189-209.
- Allman, J., Miezin, F. & McGuinness, E. (1985). Stimulus-specific responses from beyond the classical receptive field: neurophysiological mechanisms for local-global comparisons on visual neurons. *Annual Review of Neuroscience* **8**, 407-430.
- Amthor, F.R., Takahashi, E.S. & Oyster, C.W. (1989). Morphologies of rabbit retinal ganglion cells with concentric receptive fields. *Journal of Comparative Neurology* **280**(1), 72-96.
- Atick, J.J. (1992). Could information theory provide an ecological theory of sensory processing? *Network: Computation in Neural Systems* **3**, 213-251.
- Balboa, R.M., Grzywacz, N.M. (2000). The role of early lateral inhibition: more than maximizing luminance information. *Vision Research* **17**, 77– 89.
- Balboa, R.M. & Grzywacz, N.M. (2003). Power spectra and distribution of contrasts of natural images from different habitats. *Vision Research* **43**(24), 2527-2537.
- Barlow, H.B. (1953). Summation and inhibition in the frog's retina. *Journal of Physiology-London* **119**, 69–88.
- Barlow, H.B., Fitzhugh, R. & Kuffler, S.W. (1957). Change of organization in the receptive fields of the cat's retina during dark adaptation. *Journal of Physiology-London* **137**, 338–354.
- Burton, C.J. & Moorhead, I.R. (1987). Color and spatial structure in natural scenes. *Applied Optics* **26**, 157–170.

- Calvetti, D. & Reichel, L. (2004). Tikhonov regularization with a solution constraint. *Journal of Scientific Computing* **26**(1), 224-239.
- Cao, X., David, K.M. & Norberto, M.G. (2006). Weakness of surround inhibition with natural-image stimulation. *Journal of Vision* **6**(13), 43a.
- Carandini, M. & Heeger, D. (1994). Summation and division by neurons in primate visual cortex. *Science* **264**, 1333-1336.
- Chatterjee, S., Merwine, D.K., Amthor, F.R. & Grzywacz, N.M. (2007). Properties of stimulus-dependent synchrony in retinal ganglion cells. *Visual Neuroscience* **24**(6), 827-43.
- Chichilnisky, E.J. (2001). A simple white noise analysis of neuronal light responses. *Network: Computation in Neural Systems* **12**, 199–213.
- David, S.V., Vinje, W.E. & Gallant, J.L. (2004). Natural Stimulus Statistics Alter the Receptive Field Structure of V1 Neurons. *Journal of Neuroscience* **24**(31), 6991-7006.
- Devries, S.H. & Baylor, D.A. (1997). Mosaic arrangement of ganglion cell receptive fields in Rabbit Retina. *Journal of Neurophysiology* **78**(4), 2048-2060.
- Efron, B. & Tibshirani, R. (1993). *An introduction to bootstrap*. New York, NY: Chapman & Hall.
- Enroth-Cugell, C. & Lennie, P. (1975). The control of retinal ganglion cell discharge by receptive field surrounds. *Journal of Physiology-London* **247**, 551–578.
- Enroth-Cugell, C. & Robson, J.G. (1966). The contrast sensitivity of retinal ganglion cells of the cat. *Journal of Physiology-London* **187**(3), 517-552.
- Felsen, G. & Dan, Y. (2005). A natural approach to studying vision. *Nature Neuroscience* **8**, 1643–1646.

- Field, D.J. (1987). Relations between the statistics of natural images and the response properties of cortical cells. *Journal of the Optical Society of America A-Optics Image Science and Vision* **4**(12), 2379–2394.
- Grzywacz, N.M. & Koch, C. (1987). Functional Properties of Models for Direction Selectivity in the Retina. *Synapse* **1**, 417-434.
- Hubel, D.H. & Wiesel, T.N. (1962). Receptive fields, binocular interaction and functional architecture in the cat's visual cortex. *Journal of Physiology-London* **160**, 106-154.
- Kaplan, E. & Benardete, E. (2001). The dynamics of primate retinal ganglion cells. *Progress in Brain Research* **134**, 17-34.
- Koch, K., McLean, J. & Segev, R. (2006). How Much the Eye Tells the Brain. *Current Biology* **16**, 1428–1434.
- Kuffler, S.W. (1953). Discharge patterns and functional organization of the mammalian retina. *Journal of Neurophysiology* **16**, 37–68.
- Land, E.H. (1959). Color vision and the natural image part II. *Proceedings of the National Academy of Sciences of the United States of America* **45**(4), 636–644.
- Laughlin, S.B. (1981). A simple coding procedure enhances a neuron's information capacity. *Eitschrift Fur Naturforschung C – Journal of Biosciences* **36**(9-10), 910–912.
- Levick, W.R. (1967). Receptive fields and trigger features of ganglion cells in the visual streak of the rabbit's retina. *Journal of Physiology-London* **188**, 285-307.
- Marmarelis, P. & Marmarelis, V. (1978). *Analysis of Physiological Systems: The White Noise Approach*. Plenum Press, New York.
- Merwine, D.K., Amthor, F.R. & Grzywacz, N.M. (1995). Interaction between center and surround in rabbit retinal ganglion cells. *Journal of Neurophysiology* **73**, 1547-1567.

- Olshausen, B.A. & Field, D.J. (2000). Vision and the Coding of Natural Images. *American Scientist* **88**(3), 238-245.
- Olshausen, B.A. & Field, D.J. (2004). Sparse coding of sensory inputs. *Current Opinion in Neurobiology* **14**(4), 481-487.
- Peli, E. (1990). Contrast in complex images. *Journal of the Optical Society of America A-Optics Image Science and Vision* **7**(10), 2032-2040
- Poggio, T. & Reichardt, W.E. (1976). Visual control of orientation behaviour in the fly: Part 11: Towards the underlying neural interactions. *Quarterly Reviews of Biophysics* **9**, 377-438.
- Ratliff, F. (1965). *Mach bands: quantitative studies on Neural networks in the retina*. San Francisco, California: Holden-Day.
- Reid, R.C. & Alonso, J.M. (1995). Specificity of monosynaptic connections from thalamus to visual cortex. *Nature* **378**, 281–284.
- Reid, R.C., Victor, J.D. & Shapley, R.M. (1997) The use of m-sequences in the analysis of visual neurons: linear receptive field properties. *Visual Neuroscience* **14**, 1015-1027.
- Ringach, D.L., Sapiro, G. & Shapley, R. (1997). A subspace reverse-correlation technique for the study of visual neurons. *Vision Research* **37**(17), 2455-2464.
- Rockhill, R.L., Daly, F.J., MacNeil, M.A., Brown, S.P. & Masland, R.H. (2002). The Diversity of Ganglion Cells in a Mammalian Retina. *Journal of Neuroscience* **22**(9), 3831–3843.
- Rodieck, R.W. (1965). Quantitative analysis of cat retinal ganglion cell response to visual stimuli. *Vision Research* **5**, 583–601.
- Rodieck, R.W. & Stone, J. (1965). Analysis of receptive fields of cat retinal ganglion cells. *Journal of Neurophysiology* **28**(5), 832-849.
- Ruderman, D.L. & Bialek, W. (1994). Statistics of natural images: scaling in the woods. *Physical Review Letters* **73**(6), 814–817.

- Rust, N.C. & Movshon, J.A. (2005). In praise of artifice. *Nature Neuroscience* **8**, 1647 – 1650.
- Sagdullaev, B.T. & McCall, M.A. (2005). Stimulus size and intensity alter fundamental receptive-field properties of mouse retinal ganglion cells in vivo. *Visual Neuroscience* **22**(5), 649-659.
- Simoncelli, E.P. & Olshausen, B.A. (2001). Natural image statistics and neural representation. *Annual Review of Neuroscience* **24**, 1193-1216.
- Smyth, D., Willmore, B., Baker, G.E., Thompson, I.D. & Tolhurst, D.J. (2003). The receptive-field organization of simple cells in primary visual cortex of ferrets under natural scene stimulation. *Journal of Neuroscience* **23**, 4746–4759.
- Srinivasan, M.V., Laughlin, S.B. & Dubs, A. (1982). Predictive Coding: A Fresh View of Inhibition in the Retina. *Proceedings of the Royal Society of London Series B-Biological Sciences* **216**, 427-459.
- Sterling, P. (2004). How retinal circuits optimize the transfer of visual information. In: *The Visual Neurosciences*, Vol. 1 (Chalupa LM, Werner JS, eds), pp. 234–259, Cambridge, MA: MIT.
- Theunissen, F.E., Sen, K. & Doupe, A.J. (2000). Spectral-temporal receptive fields of nonlinear auditory neurons obtained using natural sounds. *Journal of Neuroscience* **20**, 2315–2331.
- Tolhurst, D.J., Tadmor, Y. & Chao, T. (1992). Amplitude spectra of natural images. *Ophthalmic and Physiological Optics* **12**, 229–232.
- Torre, V. & Poggio, T. (1978). A Synaptic Mechanism Possibly Underlying Directional Selectivity to Motion. *Proceedings of the Royal Society of London Series B-Biological Sciences* **202**, 409-416.
- van der Schaaf, A. & van Hateren, J.H. (1996). Modeling the power spectra of natural images: Statistics and information. *Vision Research* **36**, 2759–2770.

- van Hateren, J.H. & Ruderman, D.L. (1998). Independent component analysis of natural image sequences yields spatio-temporal filters similar to simple cells in primary visual cortex. *Proceedings of the Royal Society of London Series B-Biological Sciences* **265**, 2315–2320.
- Vincent, B.T. & Baddeley, R.J. (2003). Synaptic energy efficiency in retinal processing. *Vision Research* **43**, 1283-1290.
- Vinje, W.E. & Gallant, J.L. (2000). Sparse coding and decorrelation in primary visual cortex during natural vision. *Science* **287**(5456), 1273-1276.
- Willmore, B. & Smyth, D. (2003). Methods for first-order kernel estimation: simple-cell receptive fields from responses to natural scenes. *Network: Computation in Neural Systems* **14**, 553–577.